Characterization of Macroscopic Properties and Crystalline Defects in Neutron-Irradiated Silicon Carbide

Characterization of Macroscopic Properties and Crystalline Defects in Neutron-Irradiated Silicon Carbide

Toyohiko Yano*, Tadashi Maruyama* and Takayoshi Iseki**

(Received January 20, 1991)

Synopsis

Length change, mechanical properties, helium release behavior, ESR observation and microstructure of neutron-irradiated silicon carbide (SiC) were investigated. Changes in those properties due to annealing were also measured to clarify the relationship between crystalline defects induced by neutron irradiation and macroscopic properties. Firstly, the effects of sintering aids on irradiation and annealing behavior of three kinds of SiC ceramics were described. Swelling, starting temperature to decrease in length during annealing and recovery rate up to 1300°C were not affected by sintering aids. On the other hand, the bending strength and length change above 1300°C were influenced by the kind of sintering aids. Secondary, the effects of external stress on defect annihilation and bubble swelling during annealing of neutron-irradiated specimens were investigated. From those experiments, it is clarified that the decrease in length by annealing below 1300°C was not affected by the external stress. However, annealing above 1300°C led to an increase in length in B-containing SiC, and the compressive stress retarded the expansion along the loading direction. In the third section, the helium release behavior of neutron-irradiated SiC containing B was observed and it was clarified that the helium release rate of ceramic and its powder was different from each other. Defects characterization was carried out by ESR measurement and high-resolution electron microscopy. ESR signal related to the vacancy type defects having unpaired electrons markedly increased by higher fluence irradiation over $5\times10^{24}n/m^2$, and the intensity of signal decreased with increasing annealing temperature above irradiation temperature with slightly higher rate than that of length decrease. It indicated that the vacancies with unpaired electron detected by ESR selectively disappear at lower temperature than those detected by a macroscopic length measurement. High-resolution electron microscopy revealed that very small interstitial type Flank loops lying on {111}, having a Burgers vector **b**=1/3<111>, were formed in β-SiC which was heavily-neutron-irradiated in a fast reactor. Defect nuclei, a few nanometer in diameter, in hexagonal α-SiC were induced by lower doses in a thermal reactor. They are on the (0001) basal plane and have a Burgers vector **b**=1/6[0001].

---

* Research Laboratory for Nuclear Reactors, Tokyo Institute of Technology, Tokyo 152

**Department of Inorganic Materials, Faculty of Engineering, Tokyo Institute of Technology, Tokyo 152

I. Introduction

Ceramic materials have not found wide use in fission nuclear reactors with the exception of graphite moderators, SiC encapsulation of fuel elements in high temperature gas cooled reactor, oxide electrical insulators and B_4C neutron absorbers. In fusion reactors, many ceramic materials must be required in a number of areas such as first wall, radio frequency heating system window, electrical insulators at neutral beam injector, toroidal current break and direct convertor. From the stand point of safety, low activation ceramic materials are commonly desired in all radiation fields.

However there has been little study of irradiation effects in ceramics as compared with metals. In this paper, we shall summarize our recent studies on neutron-irradiated SiC, used as nuclear fuel coating in high temperature gas cooled reactor, as uninstrumented irradiation temperature monitor in thermal and fast reactors and as a candidate material for fusion reactor components, which were carried out to create the basic understandings of radiation damage.

The fabrication of SiC ceramics requires some sintering aids or special engineering techniques for sintering because their strong covalent bonding character. Physical and mechanical properties as well as microstructures of SiC ceramics are affected by their production processes and/or sintering aids. Moreover, radiation effects on the mechanical and other properties of SiC may depend on their sintering aids. Further, considering an application of SiC for fusion reactors, it is subjected to irradiation of high-energy neutrons up to 14MeV which cause not only displacement damage but also helium production from (n,α) nuclear reactions. Then, the effect of He and He release from SiC are also studied using a neutron-irradiated SiC ceramic containing ^{10}B isotope.

II. Experimental Procedure

Three types of SiC ceramics, consists of mainly α-SiC, (1) reaction-bonded SiC containing about 9% free Si (RB-SiC), (2) pressureless-sintered SiC containing about 1% B and C (PLS-SiC), and (3) hot-pressed SiC containing about 1% BeO (HP-SiC), were neutron-irradiated in the Japan Materials Testing Reactor (JMTR) under three conditions shown in Table 1 in He encapsulated containers. After irradiation, some of the specimens were annealed for 1 h at temperatures between 300 and 2000°C under vacuum. A set of specimens, one stressed and another stress free, were annealed together under vacuum in a furnace attached to an Instron type testing machine. Swelling and length change of the specimens were measured by a point type micrometer. The dimension of specimens for 4-point bending test was $4x2x25mm^3$.

The specimens for helium release measurement were PLS-SiC and irradiated to fluences of $4.5x10^{24}$, $6.0x10^{24}$, and $5.2x10^{24}n/m^2$ at 240, 650, and 840°C, respectively. After neutron irradiation, powder specimens were made by grinding the sintered specimens by diamond blade, and powders had an average particle size of about 1.2μm were obtained. The helium release rate was measured as a function of temperature using a helium detector.

A high-resolution electron microscope observation was performed on the β-SiC

specimens which were neutron-irradiated in fast-breeder reactors up to $1.0x10^{27}n/m^2$. Irradiation temperature of β-SiC specimens was around 450°C. α-SiC specimens were also inspected. An ESR signal from β-SiC polycrystals was obtained at liquid nitrogen temperature. Frequency of the oscillator was kept constant at 9.2 GHz.

III. Results and Discussion

III.1. Effects of Neutron Irradiation and Subsequent Annealing on Length and Strength of SiC Ceramics[1,2)]

Table 1 summarizes the macroscopic length changes of the three kinds of SiC specimens induced by the neutron irradiation. The increase in length by irradiation strongly depends on irradiation temperature. As the irradiation temperature increases, the length change decreases. One can also see the effect of sintering aids or minor components on the irradiation-induced length change. The increases in length of PLS- and HP-SiC are almost the same and larger than that of RB-SiC. Table 2 shows the 4-point bending strength before and after neutron irradiation ($6.0x10^{24}n/m^2$). The irradiation decreased the strength of RB- and PLS-SiC by 30 and 20%, respectively, but increased the strength of HP-SiC by 10%.

Fig. 1 shows the macroscopic length and weight changes during the isochronal annealing(1 h) of RB-SiC which was irradiated to a fluence of $8.0x10^{23}n/m^2$ at 280°C. As reported previously, the length starts to decrease near the irradiation temperature. A monotonous decrease in the length from 300 to 1300°C is due to the recombination of interstitials and vacancies, and it is not influenced by the sintering processes. After the length slightly decreases between 1300 and 1400°C, the rate of

Table 1. Length changes induced by neutron irradiation.

Neutron fluence (n/m^2) ($E>1$ MeV)	Irradiation temperature (°C)	Material	Length change (%)
8.0×10^{23}	280	RB (3) [a)]	0.51 (0.010) [b)]
		PLS (3)	0.71 (0.003)
		HP (3)	0.66 (0.009)
4.3×10^{24}	600	RB (3)	0.28 (0.018)
		PLS (3)	0.35 (0.016)
		HP (4)	0.39 (0.007)
6.0×10^{24}	640	RB (5)	0.22 (0.009)
		PLS (7)	0.32 (0.006)
		HP (7)	0.31 (0.016)

a) Number of specimens.
b) Standard deviation.

Table 2. Four-point bending strength (MPa) before and after neutron irradiation ($6.0x10^{24}n/m^2$).

Material	RB	PLS	HP
Before irradiation	530	430	360
	(28) [a)]	(34)	(28)
After irradiation	370	350	390
	(61)	(15)	(19)
Change induced by irradiation (%)	−30	−20	+10

a) Standard deviation.

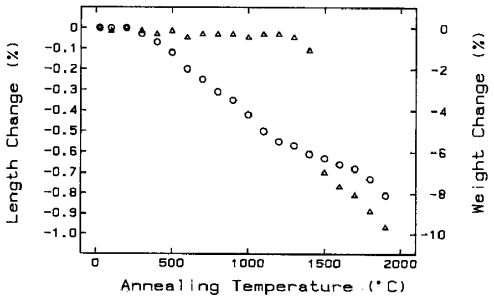

Fig. 1. Macroscopic length (circle) and weight (triangle) changes against annealing temperature for neutron-irradiated RB-SiC.

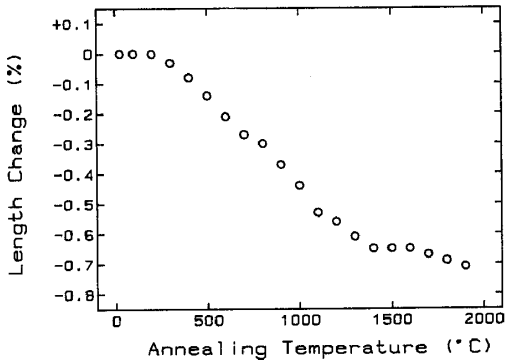

Fig. 2. Macroscopic length change against annealing temperature for neutron-irradiated HP-SiC.

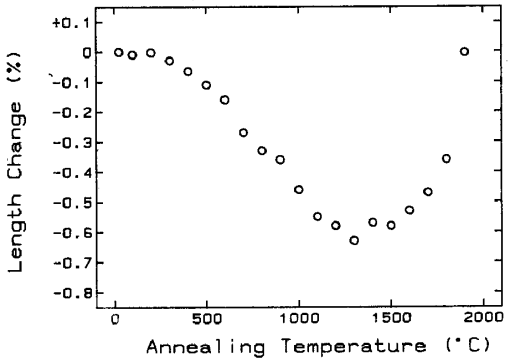

Fig. 3. Macroscopic length change against annealing temperature for neutron-irradiated PLS-SiC.

decrease again becomes fast above 1400°C. As shown in Fig. 1, an abrupt decrease in weight occurs at about 1400°C corresponding to the vaporization of Si. Then, the decrease in length above 1400°C is likely to be due to the vaporization of Si.

Fig. 2 shows the length change by annealing of HP-SiC irradiated as the same condition as Fig. 1. The contraction was almost completed at 1400°C.

Fig. 3 shows a macroscopic length change during the isochronal annealing of PLS-SiC irradiated as the same condition as Fig. 1. The coincidence between the temperature at which the length decreases and irradiation temperature is also observed. When annealing temperature is raised higher than approximately 1300°C, the length starts to increase. The increase in length by annealing above 1300°C was only observed in PLS-SiC, which contained B as a sintering aid. He atoms had been formed as a result of the nuclear reaction of $^{10}B(n,\alpha)^{7}Li$. Thus, it is natural to consider that the above length increase can be ascribed to the formation of helium bubbles, as shown in Fig. 18. The length increase by the formation of He bubbles must be an increasing function of neutron fluence, and it was confirmed from the same measurement of higher fluence specimen.

III.2. Effects of External Stress on Defect Annihilation and Bubble Swelling During Annealing of Neutron-Irradiated Silicon Carbide[3,4)]

Fig. 4. shows macroscopic length changes by isochronal annealing of HP-SiC containing 1% BeO, irradiated to a fluence of $4.5\times10^{24}n/m^2$ at 350°C. The applied compressive stress was 130 MPa. The circles indicate the data subjected to the stress, and the triangles those free from stress during annealing. Below the irradiation temperature, no change in length was observed. More importantly, it was found that the external stress did not affect the magnitude of the length change. It means that the external stress did not accelerate defect annihilation. Similar results were obtained in RB-SiC. Even an increase in stress to 560 MPa led to a similar results, as shown in Fig. 5.

As mentioned above, the annihilation of irradiation-induced defects, as detected by shrinkage, is completed by annealing about 1400°C. Except for RB- and PLS-SiC, the irradiated SiC specimens did not show a change in length by annealing

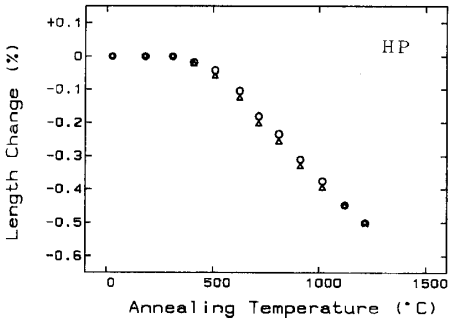

Fig. 4. Macroscopic length changes by isochronal annealing of HP-SiC. The magnitude of external stress is 130 MPa. Circle indicate the data subjected to stress, and triangle free from stress.

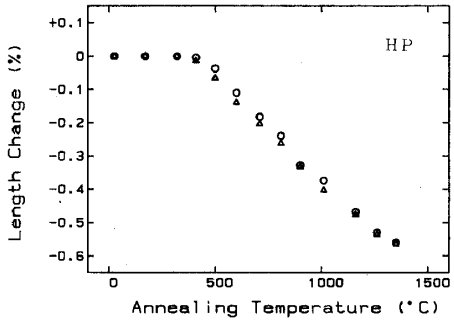

Fig. 5. Macroscopic length changes by isochronal annealing of HP-SiC with the same irradiation condition as shown in Fig. 4. The magnitude of external stress is 560 MPa.

above about 1400°C. PLS-SiC containing 1% B and C shows an increase in length (bubble swelling) by formation of He bubble at grain boundaries above about 1400°C, as shown in Fig. 18. A substantial increase in length must be attributed to the flow of thermal vacancies to He bubbles. The flow of vacancies to the existing bubbles leads to the macroscopic volume expansion as shown in Fig. 3.

Fig. 6(A) shows macroscopic length changes in the stress direction by isochronal annealing of PLS-SiC, irradiated to a fluence of $4.5 \times 10^{24} n/m^2$ at 350°C. Similarly to the results of RB- and HP-SiC, no effect of the external stress on the shrinkage was observed below 1300°C. However, the effect of external stress could be observed above 1300°C, which is the starting temperature of forming He bubbles. External stresses suppressed the expansion in the stress direction, while the stress-free specimen expanded with increasing temperature. Fig. 6(B) shows macroscopic length changes in the lateral direction of the same specimen as that of Fig. 6(A). The specimen subjected to the external stresses expanded in the lateral direction slightly more than the stress-free specimen. Similar results were obtained in the specimen irradiated to a fluence of $2.4 \times 10^{24} n/m^2$ at 700°C. This stress effect was further confirmed by applying a larger stress, 260MPa, after stress-free bubble swelling and 130 MPa-stressed bubble swelling. Fig. 7 shows macroscopic length changes for various specimens against external stress at 1600°C.

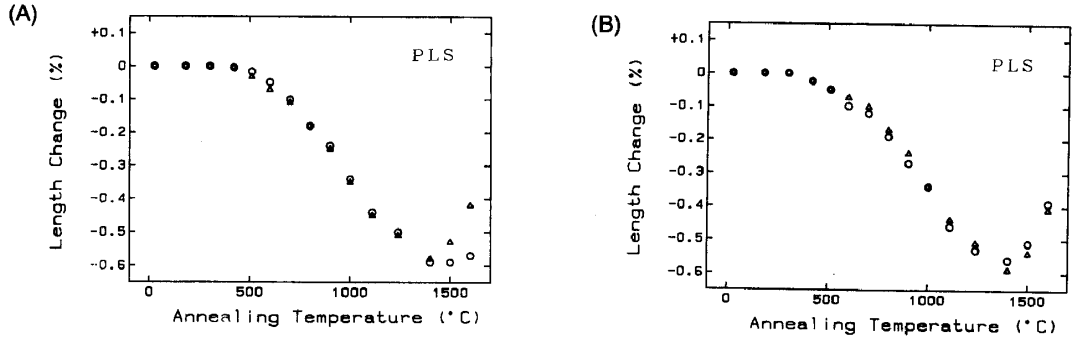

Fig. 6. (A) Macroscopic length changes by isochronal annealing in the stress direction of PLS-SiC. The magnitude of external stress is 130MPa. Circle indicates the data subjected to stress, and triangle free from stress. (B) The same specimen as that of (A), but in the lateral direction.

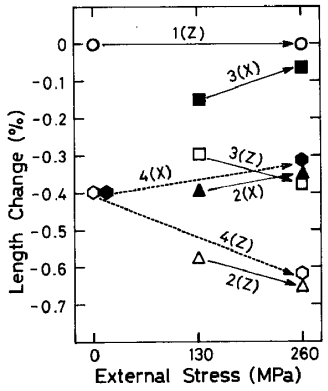

Fig. 7. Effects of external stress on the bubble swelling at 1600°C in PLS-SiC. (Z) and (X) indicate the length in the stress direction and lateral direction, respectively. The numbers 1 to 4 indicate the history of irradiation and subsequent annealing.

He bubble on a grain boundary have flat shapes, their short axis perpendicular to the grain boundary. The pressurized nonspherical bubbles produce anisotropic strains. In the case of flat bubble, the strain parallel to the short axis is larger than that perpendicular to it. Thus, a compressive stress reduces the formation of bubbles on boundaries parallel to the stress axis. This is the reason that the compressed specimens showed smaller expansion due to swelling along the loading axis, while they exhibited larger expansion along lateral direction. The change in bubble population is caused by the transport of He-vacancy complexes from the stress-unfavored to the stress-favored bubbles.

III.3. Helium Release from Neutron-Irradiated SiC Containing ^{10}B Isotope[5,6]

Fig. 8 shows the helium release rate from 1 mg of neutron irradiated SiC powder. The helium release rate increased above 800°C and two large release peaks were observed at 1100 and 1260°C in every specimen. A sharp decrease in the release rate at about 1200°C was also observed. Furthermore, small release peaks were detected at about 200 and 450°C. It is noted that the height of the release peak depends on the irradiation temperature of the specimen.

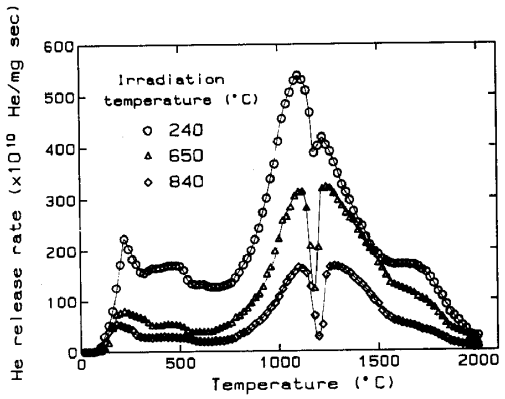

Fig. 8. Helium release rate from neutron-irradiated PLS-SiC powder with annealing at a rate of 8°C/min to 2000°C.

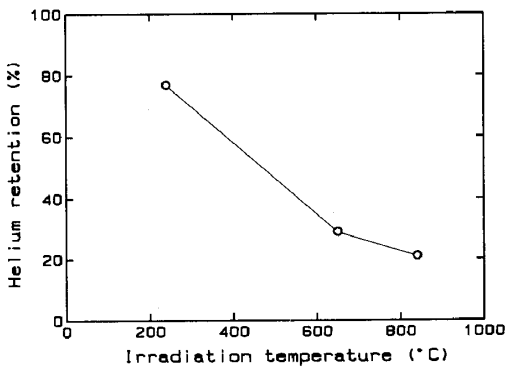

Fig. 9. The ratio of total helium retained to total helium produced in neutron-irradiated PLS-SiC.

Table 3. Irradiation conditions, and the amount of helium produced (calculated) and retained (measured) in 1 mg of neutron-irradiated PLS-SiC powder.

Irradiation temperature (°C)	Fast neutron fluence (n/m^2, $E>1$ MeV)	Total helium produced	Total helium retained
240	4.5×10^{24}	4.6×10^{16}	3.5×10^{16}
650	6.0×10^{24}	6.1×10^{16}	1.8×10^{16}
840	5.2×10^{24}	5.3×10^{16}	1.1×10^{16}

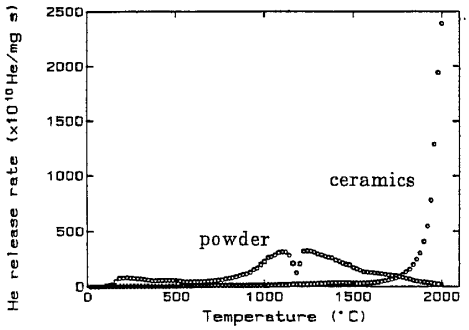

Fig. 10. Helium release rate from neutron-irradiated PLS-SiC ceramics and powder with increasing temperature at a rate of 8°C/min to 2000°C.

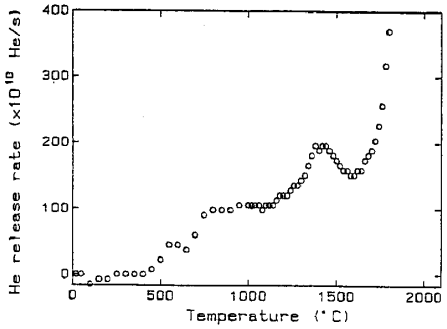

Fig. 11. Helium release rate from neutro-irradiated PLS-SiC ceramics with increasing temperature at a rate of 8°C/min to 2000°C.

Void formation in SiC is reported above 1250°C during neutron irradiation, which indicates that vacancies are not able to immigrate to form voids at low temperatures. On the other hand, calculations of the migration energy of interstitials in Si, Ge and diamond, of group IV semiconductors, the same as SiC, indicate the nearly zero interstitial migration energy. These results suggest that interstitial helium atoms can migrate very rapidly in the lattice in SiC. Therefore, we can consider a possible release mechanism that helium atoms dissociate from associated defects through activated jumping processes and are released after rapid diffusion through interstitial sites with increasing temperature. It is considered that helium release is closely related to the configuration of associated defects with helium atoms, which may have different binding energies.

Table 3 shows the total helium produced (calculated) and retained (measured) in 1 mg of SiC. Fig. 9 shows the ratio of the total helium retained to that produced as a function of irradiation temperature. The ratio decreased with increasing irradiation temperature, and the substantial portion up to 80% of helium was released from the sintered specimen during irradiation at 840°C for 1000 h.

Helium release behavior from bulk specimens($2x4x0.15mm^2$) ($6.0x10^{24}n/m^2$) is presented in Fig. 10. As contrasted with the powder specimen, the sintered specimen maintained low gas release rate up to 1800°C and exhibits a rapid increase in release rate above this temperature. Fig. 11 shows the helium release rate from a sintered specimen of size $2x4x12mm^3$ below 1800°C, more precisely.

Helium release from the sintered specimen started at 500°C and tended to increase with increasing temperature with a peak at 1400°C. However, the sintered specimen maintained a low gas release rate up to 1800°C, which is a quite different helium release behavior from that of the powder specimen. The low gas release rate up to 1800°C suggests that diffusion of helium in grains did not dominate the helium release behavior of the sintered specimen. In SiC, extensive vacancy migration can occur above 1250°C. Furthermore, since bubbles will act as trapping sites for helium

atoms if vacancies migrate together with helium atoms. It is therefore considered that helium atoms which migrated to grain boundaries are trapped to form bubbles, and consequently the release rate decreased above 1400°C to form small peaks. Bubbles at grain boundaries grew with increasing temperature as shown in Fig. 18. After annealing at 2000°C, bubbles at grain boundaries extended to form large pores and form a long-range network of pores which is open to the free surface. It is concluded that the primary mechanism of the helium release above 1800°C is the interlinkage of bubbles at grain boundaries to form pores open to the surface.

III.4. ESR Observation in Neutron-Irradiated and Annealed β-SiC[7)]

In fig. 12, changes in the intensity of the ESR signal are plotted against the neutron fluence. The irradiation temperatures for these specimens are estimated to be about 450°C. The intensity rapidly increases up to a fluence of $4.0\times10^{24}n/m^2$ and then slightly decreases with increasing neutron fluence.

Fig. 13 shows an intensity change of the ESR signal by isochronal annealing in the specimen irradiated to a fluence of $4.0\times10^{24}n/m^2$. The intensity started to decrease from around the irradiation temperature. This is because that recombination between vacancies and interstitials occurs above the irradiation temperature. Correspondingly, the number of unpaired electrons also starts to decrease above the irradiation temperature. It is seen that a decrease in the intensity became less above 900°C in this specimen.

As shown in Fig. 2, a decrease in macroscopic length by isochronal annealing in irradiate SiC specimens continued to about 1400°C. This indicates that some vacancies produced by neutron irradiation must have remained in SiC up to about 1400°C. On the other hand, the intensity decrease of the ESR signal in these specimens almost saturated at 700-900°C. Thus, vacancies with unpaired electrons detected by ESR selectively disappear at lower temperatures than those detected by a macroscopic length change.

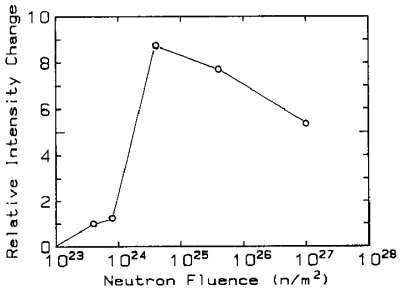

Fig. 12. Relative intensity change of ESR absorption curves of β-SiC normalized by the value of $4.0\times10^{23}n/m^2$ against neutron fluence.

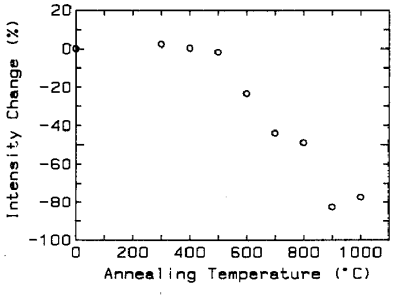

Fig. 13. Changes in the intensity against the annealing temperature in β-SiC specimen.

III.5. Electron Microscopy of Neutron-Irradiated SiC[6,8,9]

Typical dark-field micrographs of heavily neutron-irradiated β-SiC taken along the <110> incident beam direction are shown in Fig. 14. Many short lines orientated in two directions are seen. The lines are parallel or at an angle of 70° to the stacking fault frequently observed in β-SiC, of which the fault vector is known to be R=1/3<111>{111}. Then the loops lie on {111} planes and are viewed edge on.

Fig. 15 shows a high-resolution image of a thinner portion of the specimen including a loop. The photograph was taken under the <110> axial illumination condition. The layer distance along the vertical direction is 0.25nm, which corresponds to the height of a SiC_4 tetrahedron, that is the height of a unit sheet stacked along the <111> direction. The arrangement of the dots shows the existence of a single extra layer between the black arrows marked in the figure. The array of black dots across the extra layer kinked twice between the arrows, as indicated by small white dots and small white arrows.

Dislocation models for zincblende-type crystals were discussed by Clinard and Hobbs[10], by analogy to the loop configuration in BeO. A single layer loop is constructed by insertion of a single rotated layer between an originally existing layer, creating two modified layers. For the ABCA stacking sequence, B' plus the inserted layer create C'B', yielding the sequence CA|C'B'|CA, where the prime denotes a π rotation of the tetrahedral unit. Fig. 16(b) represents this stacking sequence model, as compared with a perfect crystal shown in Fig. 16(a). Lattice images were calculated by a multislice method. It was determined that the atomic configuration of the loops may be determined as the model presented in Fig. 16(b) rather than the model in Fig. 16(c). Then the Burgers vector of the loop is 1/3<111>{111}. These loops were induced by heavy neutron irradiation doses of above approximately $5x10^{26}n/m^2$ in a fast reactor.

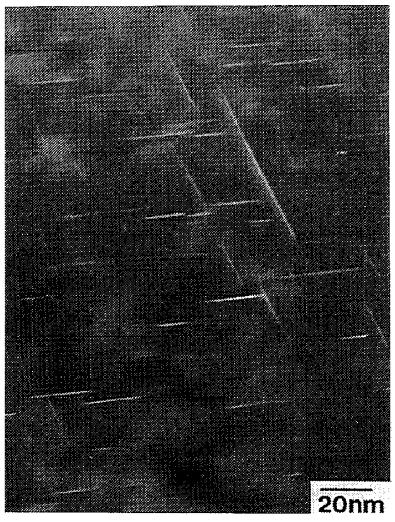

Fig. 14. Dark-field photograph of the neutron-irradiated β-SiC taken along <110> incident beam direction. The neutron dose was $1.0x10^{27}n/m^2$ and the irradiation temperature 640°C.

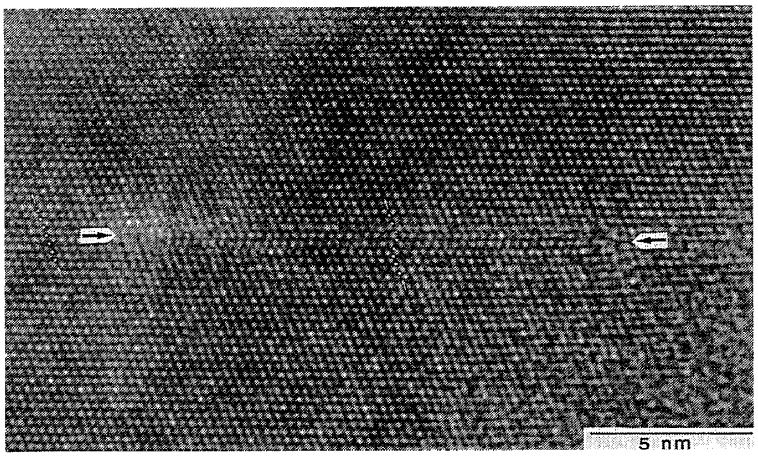

Fig. 15. [110] lattice image of the same specimen as fig. 14. The arrangement of the dots shows the existence of a single extra layer between the black arrows.

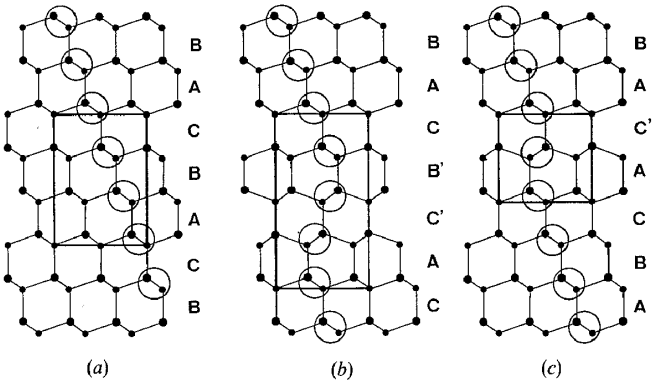

Fig. 16.

Structure models of (a) a perfect and (b), (c) a faulted crystal viewed along the axis corresponding to the cubic <110> directions. The stacking sequence of SiC_4 tetrahedra is indicated by the letters ABC and A'B'C', where the prime shows a π rotation of the SiC_4 tetrahedral unit.

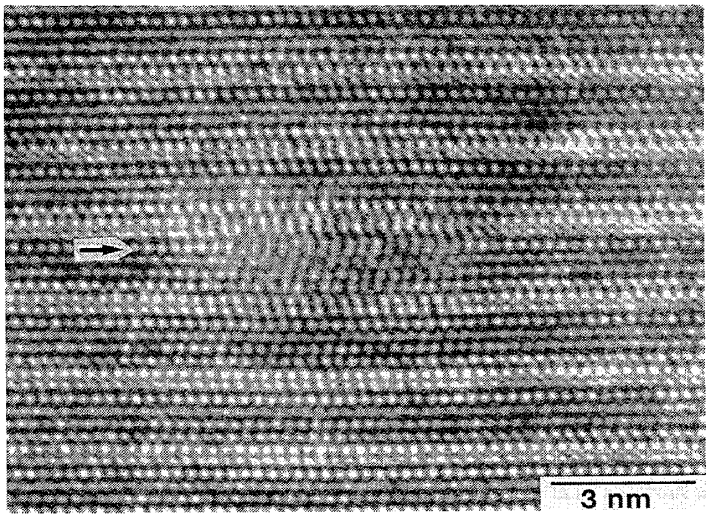

Fig. 17.

[$11\bar{2}0$] lattice images of HP-SiC irradiated to $1.3 \times 10^{25} n/m^2$ at 640°C and annealed at 1400°C for 1 h. The arrays of dots parallel to the (0001) plane are modulated at the point arrowed in the figure, showing nuclei of interstitial loops.

Defect nuclei a few nanometers in diameter in hexagonal α-SiC were induced by lower doses in a thermal reactor($2 \times 10^{25} n/m^2$). They are on the (0001) basal plane and have a Burgers vector **b**=1/6[0001], as shown in Fig. 17.

Both density and size of the loop did not change up to 1000°C, but the linear dimension began to shrink at around irradiation temperature. Moreover, enlarged loops remained after annealing at 1400°C, at which the neutron irradiation induced swelling is almost annealed out. The results suggest that the dislocation loops observed by HREM are not the cause of irradiation-induced swelling of SiC.

Fig. 18 shows the results of TEM observations around grain boundaries of PLS-SiC annealed at 1200, 1400, 1600 and 2000°C. Only "black spot" defects were observed in the specimen annealed at 1200°C. In the specimen annealed at 1400°C, helium bubbles having a size of about 5 nm were observed and uniformly distributed along grain boundaries. Helium bubbles grew in size to 30 nm and had a lenticular shape after annealing at 1600°C. In the specimen annealed at 2000°C, almost all the bubbles were interlinkaged and extended to form large pores. These result indicates that the formation of helium bubbles at grain boundaries begins at around 1400°C, but the release of helium from the bulk specimen mainly due to the formation of interlinked pores after annealing in the temperature range 1800-2000°C.

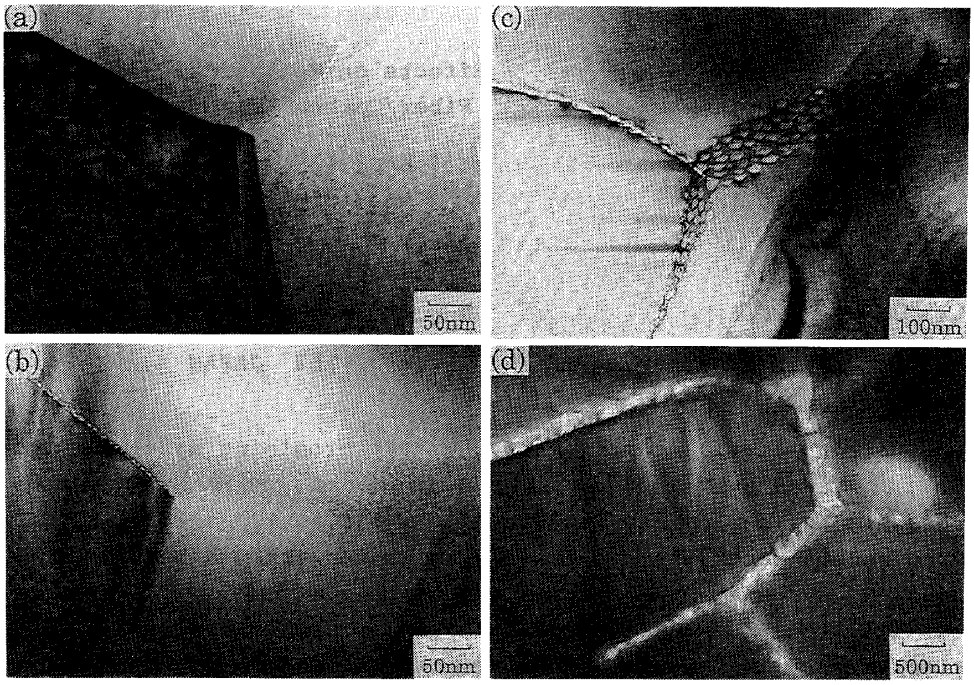

Fig. 18. TEM photographs of neutron-irradiated PLS-SiC ceramics, irradiated to $6.0 \times 10^{24} n/m^2$ at 650°C, annealed for 0 min at (a)1200°C, (b)1400°C, (c)1600°C and (d)2000°C.

IV. Summary

Neutron-irradiated SiC crystal contains several type of crystalline defects. One is vacancies and interstitials (Frenkel defect and clusters), and the other very small interstitial dislocation loops. Most of the Frenkel pairs are annihilated during the irradiation. Higher irradiation temperature, higher annihilation rate. Some portion of remained interstitials and vacancies may associate to impurities or crystal defects originally existed in crystal with very wide range of binding energy. The amount of swelling directly related to the Frenkel defects remains in the crystal. Furthermore, the difference between radiation damage of SiC and that of second phases can affect to the bulk properties of SiC ceramics. Except for heavily irradiation over $5 \times 10^{26} n/m^2$, the dominant defect may be Frenkel pairs.

Post-irradiation annealing causes recovery of those defects. Interstitial atoms can migrate even at near room temperature, though vacancies can migrate only at temperatures over 1200°C at a considerable rate. Interstitial dislocation loops slightly expand after an annealing at 1400°C. Annealing below irradiation temperature is not effective to annihilation of the remained defects, because the defects which can move below that temperature already recombined during irradiation, mainly by interstitial migration process. Annealing above irradiation temperature but below around 1200°C promotes the migration of interstitials which associate to the crystal lattice with some binding energy, and annihilates with vacancies, which is immobile at that temperature. The process causes shrinkage of macroscopic length, and recovery of point defects-related properties such as thermal diffusivity. Annealing at higher

temperature leads larger amount of annihilation and length shrinkage. An external stress does not affect the recombination process. It is known that the isochronal annealing with increasing temperature gives monotonous recovery in macroscopic length. This indicates that the state of interstitials and/or vacancies in crystal is not simple and can be taken very wide variations of configurations. We can indicate that there are two types of vacancies, one is associated to unpaired electrons and one not associated to unpaired electrons. The former vacancies annihilate at lower temperature than the latter. The recombination of vacancies and interstitials is mostly completed at 1400°C annealing. But the interstitial loops remains at that temperature.

The ratio of retained helium to produced helium in SiC is decreases with increasing irradiation temperature. If the crystal containing helium atoms after neutron irradiation, helium interstitials starts to migrate through crystal lattice at near 200°C and the migration is accelerated above 800°C. Helium release behavior indicates that interstitial helium atoms are associated to defects such as vacancies, of which configuration is very complex. If the annealing temperature is raised up to around 1400°C, the migration of vacancies is progressed to formed helium bubble at grain boundary in the case of polycrystalline specimen, and causes expansion of macroscopic length. An external compressive stress retards the expansion of specimen parallel to the stress direction. The helium release from this specimen is accelerated above 1800°C by interlinkage of grain boundary bubbles.

Acknowledgements

We wish to thank the staff of the Oarai Branch, Institute of Materials Research, Tohoku University, for their helpful assistance both to the irradiation of the specimens and in the handling of the irradiated specimens.

References

(1) T. Iseki, T. Maruyama, T. Yano and T. Suzuki, J. Nucl. Mater., 170 (1990) 95.
(2) T. Suzuki, T. Yano, T. Maruyama, T. Iseki and T. Mori, J. Nucl. Mater. 165 (1989) 247.
(3) T. Suzuki, T. Yano, T. Iseki and T. Mori, J. Am. Ceram. Soc., 73 (1990) 2435.
(4) T. Suzuki, T. Iseki, T. Mori and J. H. Evans, J. Nucl. Mater., 170 (1990) 113.
(5) K. Sasaki, T. Maruyama and T. Iseki, J. Nucl. Mater., 168 (1989) 349.
(6) K. Sasaki, T. Yano, T. Maruyama and T. Iseki, J. Nucl. Mater., 176 (1990) in printing.
(7) S. Kasahara, T. Suzuki, T. Maruyama, T. Iseki, H. Kawazoe, M. Ito, J. Nucl. Mater., 161 (1989) 261.
(8) T. Yano, T. Suzuki, T. Maruyama and T. Iseki, J. Nucl. Mater., 155-157 (1988) 311.
(9) T. Yano and T. Iseki, Philos. Mag. A, 62 (1990) 421.
(10) F. W. Clinard, Jr and L. W. Hobbs, in 'Physics of Radiation Effects in Crystals' (Amsterdam, Elsevier, 1986), p.387.